Surface conduction electron emission in palladium hydrogenation nanogaps

2008 J. Phys. D: Appl. Phys. 41 085301

(http://iopscience.iop.org/0022-3727/41/8/085301)

IOP PUBLISHING JOURNAL OF PHYSICS D: APPLIED PHYSICS

J. Phys. D: Appl. Phys. **41** (2008) 085301 (6pp) doi:10.1088/0022-3727/41/8/085301

Surface conduction electron emission in palladium hydrogenation nanogaps

Yiming Li[1] **and Hsiang-Yu Lo**

Department of Communication Engineering, National Chiao Tung University, 1001 Ta-Hsueh Road, Hsinchu City, Hsinchu 300, Taiwan

E-mail: ymli@faculty.nctu.edu.tw

Received 11 October 2007, in final form 4 February 2008
Published 5 March 2008
Online at stacks.iop.org/JPhysD/41/085301

Abstract

A nanometre scale gap (nanogap) structure in palladium strip fabricated by hydrogen absorption under high-pressure treatment was proposed and applied to the surface conduction electron emitter for flat panel displays. In this paper we demonstrate that the structure possesses different high field-emission efficiencies with low turn-on voltages and high focused capability, compared with the conventional type. An experimentally validated simulation is conducted to investigate the field-emission characteristics of the explored structure. It is observed the inclined sidewall and protrusion of this nanogap can enhance the local electric field and the focused capability and protect emission areas from being damaged by impurity ions during field-emission operation. This study benefits the advanced design of metallic electrodes in nanodevice technology for new types of electron sources and display applications.

(Some figures in this article are in colour only in the electronic version)

1. Introduction

Nanometre scale gaps (nanogaps) have shown great promise as electrodes in molecular electronics [1,2], biosensors [3] and vacuum microelectronics [4]. However, most relevant research on nanogaps is only in its infancy because of the complexity and unreliability of nanogap fabrication and manipulation of nanosized constituents. One of the emerging applications of nanogaps is the surface conduction electron emitter (SCE) for flat panel displays (FPDs), which has attracted much attention since being reported by Sakai *et al* [5]. The surface conduction electron-emitter display (SED) is an advanced type of FPD based upon SCEs. Potentially, SCEs as field-emission sources are superior to conventional cathodes in many respects. These SEDs possess high quality image, quick response time as well as low power consumption [5,6], where the emission efficiency is determined by the shape and material of the SCE. The key to the SCEs at the heart of the SED is a nanometre scale gap made from ultrafine-particle film between the two electrodes. Electrons are emitted from one side of the electrode under lower driving voltage (near 15–60 V). Some of these electrons are scattered at the other side of the electrode and accelerated by the voltage (approximately 3 kV) applied between the anode and cathode, and they collide with the fluorescent-coated glass plate, causing light to be emitted. Due to the particular mechanism of the SCE device, no other focusing structure is required. Thus the efficiency of field emission is determined by both the morphology and material of the SCE. Recently, Tsai *et al* [7] have succeeded in fabricating a new type of SCE device using hydrogen absorption under high-pressure treatment. A well-defined gap size and simple process can be given by this method which is accompanied by extensive atomic migration during the hydrogen treatment. The break in the palladium (Pd) electrode results in a drastic difference around the geometric shape of the two edges of the nanogap [7]. However, studies of field-emission characteristics on this type of structure are still unclear.

As shown in the previous report [8], electron trajectories in a SED are analysed based on the multiple scattering model. Besides calculating electron beam spot on the phosphor by the Monte-Carlo ray tracing method, simple formulations for calculating beam spot size and electron-emission efficiency are proposed by Okuda *et al* [8]. Unfortunately, this model is only valid in an emitter with a coplanar cathode and a simulation that includes full three-dimensional (3D) fields and charged particles has not been considered for the electron emission of SED yet. In this work, we provide a structural analysis of the new type of SCE and demonstrate rather different electron-emission properties with its high electron-emission efficiency

[1] Author to whom any correspondence should be addressed.

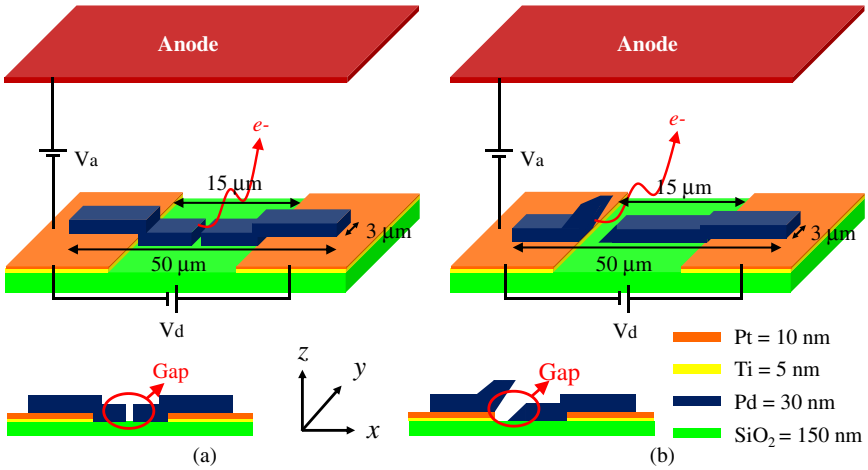

Figure 1. Schematic plot of the SED structures and the cross sections of the SCEs on the *xz* plane. The SCE in (*a*) is formed by the FIB technique and in (*b*) is fabricated by a high-pressure hydrogen absorption treatment. The thickness of this device is shown at the bottom-right corner.

and high focusing capability compared with the conventional type. The 3D finite-difference time-domain particle-in-cell (FDTD-PIC) method which combines Maxwell's equations with Lorentz's equation is employed in our simulation. The use of fundamental equations often contains the full nonlinear effects, and space charge and other collective effects can be included self-consistently by coupling charged particles to the field equations via source terms. Consequently, the program which has calibrated the theoretical model with the experimental data is developed to evaluate the field-emission characteristics of SED devices.

This paper is organized as follows. The model and calculation technique are described in section 2. In section 3, we discuss the results and field-emission mechanism of the hydrogenation fabricated SCE structure. The results of the numerical simulation will be compared with the experimental measurements. Finally, we draw conclusions.

2. Theoretical model and method of calculation

The configuration of two (conventional and proposed) types of SEDs and the cross section of SCE devices in this study are shown in figure 1. The SCEs depicted in figures 1(*a*) and (*b*) are labelled SCE I (conventional type) and SCE II (proposed) and used for the electron-emission experiments. For the SCE I device, the emitter has a coplanar structure with a Pd nanogap, which can be fabricated by the focused ion beam (FIB) technique, so that a nanogap with 25 nm separation can be obtained [9]. For the novel nanogap, it is fabricated by hydrogen absorption under high-pressure treatment. It is known that for a system under tensile stress, the defects are often near singular strain points, such as step edge or crack tips. Therefore, a Pd thin-film strip with a height difference is designed to create a step edge, and then high-pressure hydrogen treatment is used to form the nanometre scale gaps. Once Pd is exposed to hydrogen gas, adsorbed hydrogen atoms can quickly diffuse into the Pd lattice and occupy the interstitial sites. Therefore, crack initiation in the Pd thin film in the step region due to a high degree of stress concentration can result in the rupture of the Pd strip along the step edge via the process of stress relaxation through atomic diffusion driven by the stress gradient. The nanogap formed at 25 °C is approximately 25 nm wide, and other widths of nanogaps are prepared at different temperatures. The detailed fabrication process and SEM images of this structure can be found in [7]. From figure 1(*b*), we can find that the Pd electrode protrudes along the gap edge on the side with Pt/Ti underlayer and exhibits a jagged feature on the other side with a gradual film thinning towards the edge.

To explore the electron-emission properties in SCEs, FDTD-PIC simulation technique is used. Maxwell's equations and the relativistic Lorentz equation are sufficiently general that they are virtually never called into question in the electromagnetic PIC approach. However, since most physical problems involve fields defined continuously over space and an astronomical number of particles, the challenge is to achieve valid solutions with finite computational resources. The detailed FDTD-PIC method can be found in the literature [10–12] and this method used in the field-emission simulation has been explained in previous work [12,13]. Therefore, in this section, only the essential features of the method are briefly described.

In the PIC scheme, the numerical solver performs a time integration of Faraday's law, Ampere's law and the particle force equation:

$$\frac{\partial \boldsymbol{B}}{\partial t} = -\nabla \times \boldsymbol{E}, \tag{1}$$

$$\frac{\partial \boldsymbol{E}}{\partial t} = -\frac{\boldsymbol{J}}{\varepsilon} + \frac{1}{\mu\varepsilon}\nabla \times \boldsymbol{B}, \tag{2}$$

$$\frac{\partial \boldsymbol{v}}{\partial t} = \frac{\boldsymbol{F}}{m} = \frac{q}{m}(\boldsymbol{E} + \boldsymbol{v} \times \boldsymbol{B}) \tag{3}$$

and

$$\frac{\partial \boldsymbol{x}}{\partial t} = \boldsymbol{v}, \tag{4}$$

subject to constraints provided by Gauss's law and the corresponding rule for the divergence of $\boldsymbol{B}$:

$$\nabla \cdot \boldsymbol{E} = \frac{\rho}{\varepsilon} \tag{5}$$

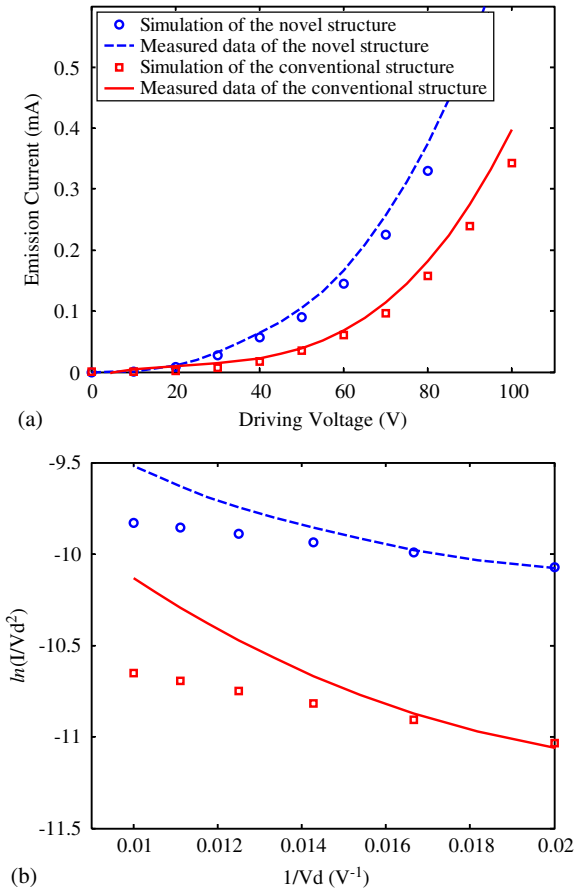

Figure 2. (*a*) *I*–*V* characteristics of these two SCEs with 25 nm wide nanogap. (*b*) Corresponding F–N plot, indicating the true nature of field emission.

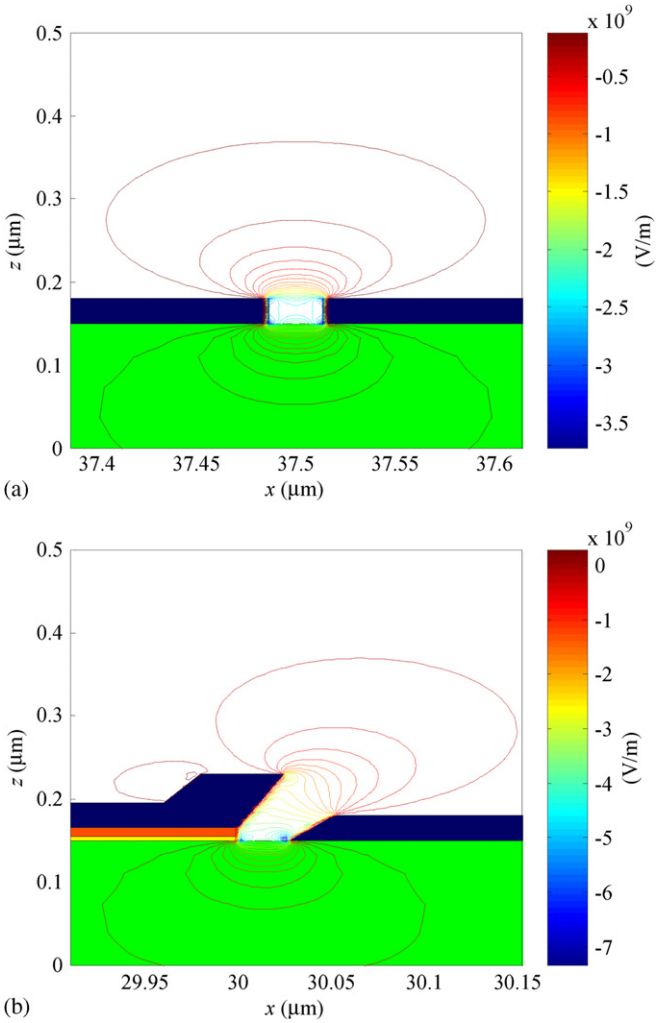

Figure 3. Contour plots of electric fields near the 25 nm wide nanogaps for conventional and novel structures. The driving voltage is fixed at 60 V.

and

$$\nabla \cdot \boldsymbol{B} = 0. \tag{6}$$

In the above equations, $\boldsymbol{E}$ and $\boldsymbol{B}$ are the electric and magnetic fields, $\boldsymbol{x}$ and $\boldsymbol{v}$ are the position and velocities of a charged particle, $\boldsymbol{J}$ and ρ are the current density and charge density resulting from those particles, μ and ε are the permeability and permittivity of free space, q is the charge of a particle and m is the mass of an electron. This time integration is usually referred to as time-domain solution. The time-integration scheme is based upon a fixed time interval between variable updates, such that the time derivatives of equations (1)–(4) are approximated in finite-difference form. The most commonly used integration scheme is the leap-frog scheme which is second order accurate and has a numerical error vanishing when $\Delta t \rightarrow 0$ [10]. The emission current density is determined by the Fowler–Nordheim (F–N) equation [14] as

$$J = \frac{AE^2}{\varphi t^2} \exp\left(\frac{-Bv\,(y)\,\varphi^{3/2}}{E}\right), \tag{7}$$

where A and B are the fitting parameters, E is the normal component of the electric field at the emitter surface, φ is the work function of the emitter material, t^2 is taken as approximately 1.1 and $v(y) = 0.95 - y^2$ with $y = 3.79 \times 10^{-5} \times E^{1/2}/\phi$ in SI units. Initially, the electrostatic field along the emitter surface is determined for a given geometry and applied voltage. The emission current density is determined by equation (7) according to the local electric field, work function of the emitter material and two fitting parameters. The simulation proceeds by pushing the emitted electrons, weighting the current and charge densities to the grids, updating the electromagnetic fields by solving equations (1) and (2) and equations (5) and (6), and then the charge particles are moved according to equations (3) and (4) using the advanced fields. These processes are repeated for each time step until the specified number of time steps is reached. The accuracy of the simulation technique was confirmed by calibrating simulated results with measurements on an experimentally fabricated 25 nm wide SCE device [15]. In the simulation, the space-charge effects are automatically included in this algorithm and all dimensions are set the same as those in the experiment.

3. Results and discussion

The electron-emission properties and distinctions of two individual surface conduction electron emitters are

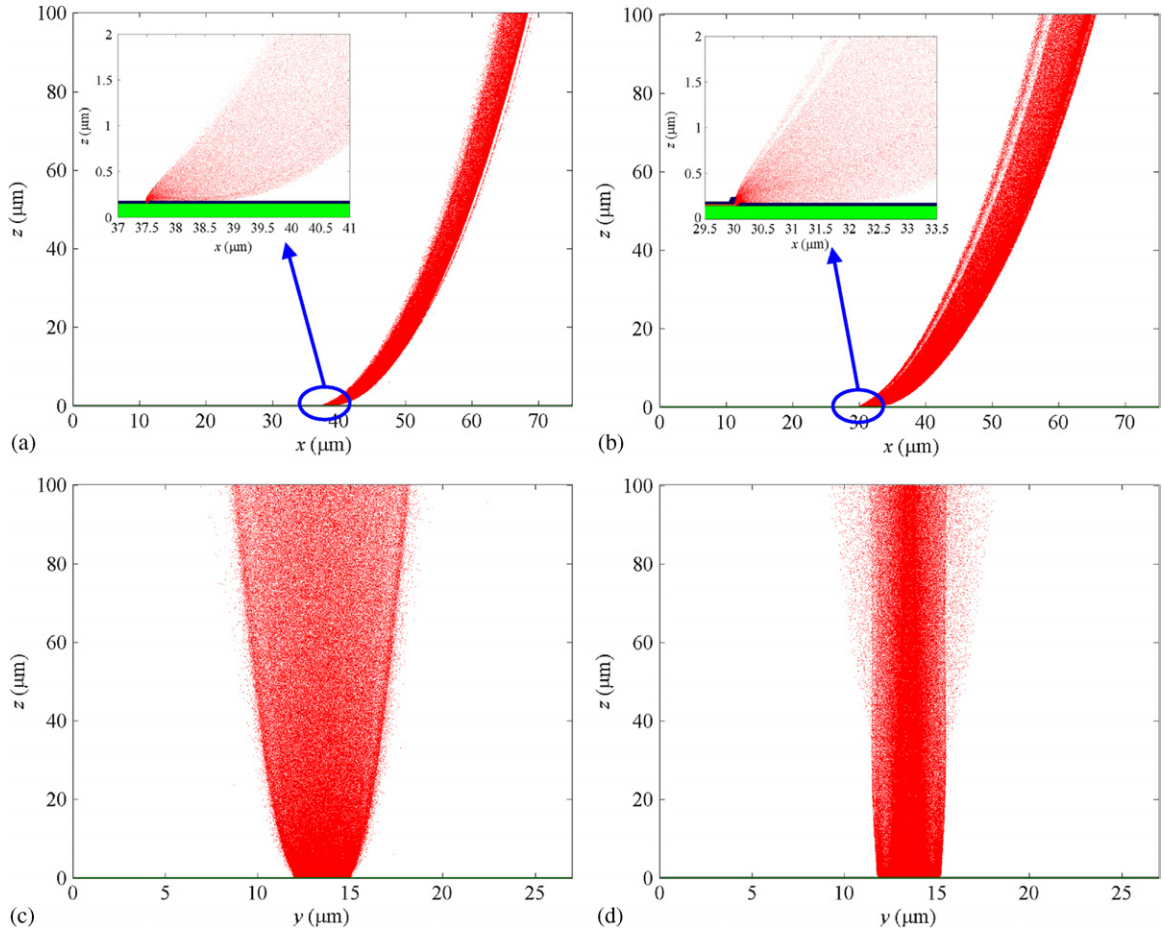

Figure 4. Electron-emission behaviour of SCE I (shown in plots (*a*) and (*c*)) and SCE II (plots of (*b*) and (*d*)). (*a*) and (*b*) are the electron beams ejected from the SCEs on the *xz* plane, where $V_d = 60$ V and $V_a = 3$ kV. (*c*) and (*d*) are the electron beams observed on the *yz* plane.

characterized by the following aspects: (1) recording of the current–voltage (I–V) curves and (2) recording of the focusing capability of the emitted electron beam and showing the emission patterns. The electron conduction characteristics of SCEs in the experiments are studied by a Keithley 237 measurement system under a vacuum condition of 5.0×10^{-6} Torr. Figure 2(*a*) shows the measured (line) and simulated (symbol) I–V characteristics of different structures of SCE with respect to the 25 nm wide nanogap. The emission current in SCE II is higher than that of SCE I through both the experiment and simulation. It shows that the proposed structure exhibits high electron emission current compared with the conventional type. A very high emission current of 0.3 mA is estimated when the driving voltage = 70 V for the 25 nm wide SCE II. The electric fields around the nanogaps, shown in figures 3(*a*) and (*b*), confirm the predictions and experimental results. We can find the SCE II having a tip around the corner on the left electrode implies that it can produce high electric fields around the emitter apex, and generate high emission current. Figure 2(*b*) shows the corresponding F–N plot of the field emission of a Pd SCE. We note that all surfaces are assumed to be smooth on the cell level in the 3D simulation, and thus calculate the electron emission by the F–N model. However, the surfaces of the nanogap may be rough due to the formation of the ductile nature. Assuming the work function $\varphi = 5.12$ eV for Pd [16], the linear relationships in the high voltage region indicate that the electron conduction followed the F–N field-emission mechanism. We note that accurate determination of current is difficult, because the calculation of local-geometric-enhanced electric field at the emitting surface is difficult and the work function may vary significantly over an atomic scale. The F–N theory considers the 1D problem with a potential profile that accounts only for image force. Thus, the atomic-scale surface roughness and the variation of the work function between different faces do not result in a significant deviation from the results obtained with the 1D description. The influence of emitter nonplanarity upon the barrier shape was reported by He *et al* [17]. At high voltages, the current density for the nonplanar model increases more slowly with the driving voltage, but its magnitude is significantly greater than the current of the planar model under the same driving voltage. The simulation results and nonplanar geometries in the measured data are shown in figure 2(*b*). Assuming the planar model in the simulation, the magnitude of emission current is indeed lower than the experimental data of the realistic nonplanar structure.

A second important aspect of the field emission is the focusing of the emitted electron beam. Electrons emitted from SCEs at a driving voltage (V_d) biased between a pair of electrodes are accelerated by an anode voltage (V_a). The

electron beam emits towards the driving electrode and goes upwards to the anode. The field emission in the surface conduction electron emitter is different from another field-emission mechanism focused on the carbon nanotubes (CNTs) [18] as the electron sources. The vertically aligned CNTs grown in patterned areas are used as electron sources in the field-emission displays, but detrimental electron beam spreading may occur in vacuum space. Thus, the typical emitter structure with a driving electrode is proposed for focusing and extracting the electron beams. It contrasts with the SED structure which has no focused electrode; for this reason, the field-emission efficiency and the emitted electron beam are determined by both the morphology and material of SCE. Figures 4(*a*) and (*b*) show the two electron trajectories of the cross section on the *xz* plane. It is found that the electron beams spreading in the two SCEs on the *xz* plane are similar and cannot investigate the advantage of the proposed structure. Zoom-in plots around the emitters, shown in the insets of figures 4(*a*) and (*b*), illustrate the mechanisms of electron emission in SCEs. Two electron beams of the cross section on the *yz* plane are shown in figures 4(*c*) and (*d*); the focusing capability in the SCE II is better, compared with SCE I. With the 3 μm wide Pd strip, the width of the electron beam on the anode is approximately 3 μm in SCE II. The electric field in the vacuum causes the electrons tunnelling into vacuum to fall onto the driving electrode surface. When the structure of the nanogap in SCE I is planar, a large fraction of the electrons emitted into vacuum may first have collisions with the driving electrode and again be elastically scattered back into vacuum. Then, electrons after the elastic scattering by the driving electrode will be attracted by the anode voltage and move upwards. Therefore, the width of the electron beam becomes larger on the anode plate due to the electrons of elastic scattering. The structure of nanogap that we proposed for SCE contrasts to that of the SCE I in the planar nanogap. Because of the height difference and the inclined sidewall around the nanogap, it can increase the electric field around the nanogap to obtain higher emission current. A few of the emitted electrons will directly collide with the driving electrode due to the stepped structure. Figures 5(*a*) and (*b*) show distributions of the current density on the anode plate. If the divergence of an electron beam is serious, the spot size is too large and the resolution is poor. The current density of the electron beam amounts to 25 μA μm^{-2} in SCE II and is higher than SCE I compared with figure 5(*a*). We observe that the proposed structure improves the focusing of the electron beam from figures 5(*a*) and (*b*). Therefore, it is possible to obtain good brightness and high resolution at this moment. To illustrate the potential of this novel SCE device for display applications, the image of a light spot is produced, shown in [7], on a phosphor plate when driving voltage = 50 V, which is 500 μm away from the emitter and $V_a = 2.5$ kV with respect to the cathode. It is worthwhile noting that electrons can actually emit towards the driving side from any part of the inclined sidewall of the protruding cathode and move upwards to the phosphor plate by the collection of anode voltage. The stepped and inclined nanogap has several advantages over the conventional planar nanogap. The inclined sidewall of the cathode may function as a shield protecting electron-emitting areas from being struck by impurity ions, which are accelerated vertically in the high electric field between the cathode and the anode.

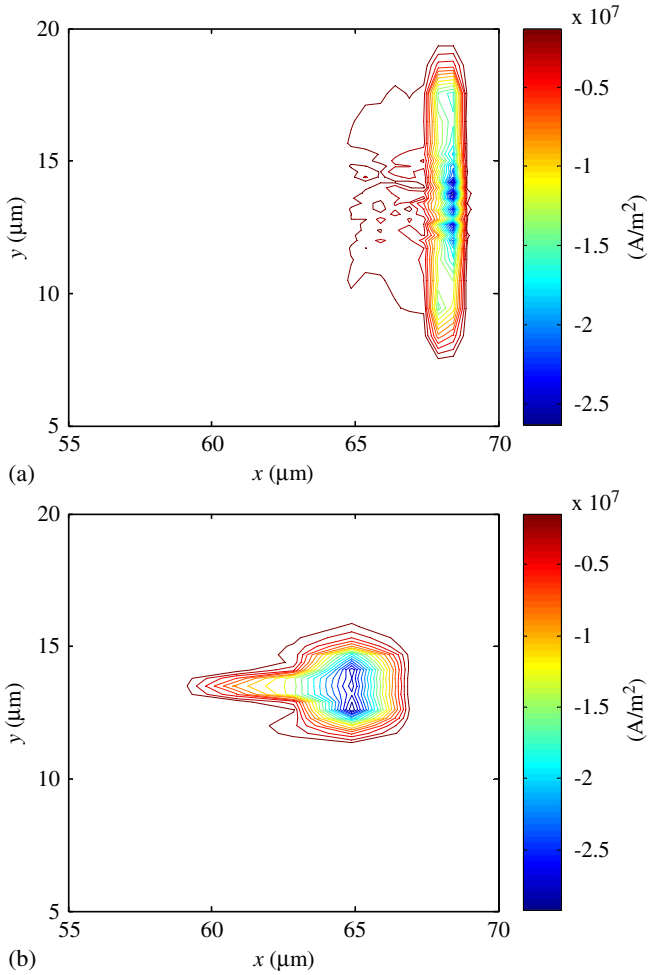

Figure 5. Simulated current density distributions on anode plates for (*a*) SCE I and (*b*) SCE II. They show that the focusing capability in SCE II is better than in SCE I.

4. Conclusions

Investigation of the electron-emission properties of the proposed structure fabricated by high-pressure hydrogen absorption treatment has been performed by numerical simulation and experiments. The electron emission of this SCE structure exhibited nonplanar F–N-like emission behaviour and high emission current, compared with the conventional structure. The nanogap which is fabricated by the high-pressure hydrogen absorption treatment has a protrusion on the cathode and an inclined sidewall, and these features can enhance the local electric field and the focused capability and protect emission areas from being damaged by impurity ions during the field-emission operation. Using the proposed nanogap, it is also easy to build pairs of electrodes for contacts to nanometre scale species, with significant potential applications of the electron sources to field-emission displays. Advanced applications using this kind of nanogap structure

are now under consideration, including molecular devices and chemical sensors.

Acknowledgments

This work was supported in part by the Taiwan National Science Council (NSC) under Contracts NSC-96-2221-E-009-210, NSC-95-2221-E-009-336, NSC-96-2752-E-009-003-PAE, NSC-95-2752-E-009-003-PAE, by MoE ATU Program, Taiwan, under a 2006–2007 grant, and by Chunghwa Picture Tubes under a 2006–2008 grant.

References

[1] Reed M A, Zhou C, Muller C J, Burgin T P and Tour J M 1997 *Science* **278** 252–4
[2] Linag W, Shores M P, Bockrath M, Long J R and Park H 2002 *Nature* **417** 725–9
[3] Yi M, Jeong K H and Lee L P 2004 *Biosens. Bioelectron.* **20** 1320–6
[4] Lee H I, Park S S, Park D I, Ham S H and Lee J H 1998 *J. Vac. Sci. Technol.* B **16** 762–4
[5] Sakai K, Nomura I, Yamaguchi E, Yamanobe M, Ikeda S, Hara T, Hatanaka K, Osada Y, Yamamoto H and Nakagiri T 1996 *Proc. EuroDisplay '96 (Birmingham, UK)* pp 569–72
[6] Yamaguchi E, Sakai K, Nomura I, Ono T, Yamanobe M, Abe N, Hara T, Hatanaka K, Osada Y, Yamamoto H and Nakagiri T 1997 *J. Soc. Inform. Display* **5** 345–8
[7] Tsai C H, Pan F M, Chen K J, Wei C Y, Liu M and Mo C N 2007 *Appl. Phys. Lett.* **90** 163115-7
[8] Okuda M, Matsutani S, Asai A, Yamano A, Hatanaka K, Hara T and Nakagiri T 1998 *SID Symp. Dig. (Anaheim, CA)* 185–8
[9] Tsai C H, Chen K J, Pan F M, Lo H Y, Li Y, Liu M and Mo C N 2007 *SID Symp. Dig. (Long Beach, CA)* 583–5
[10] Birdsall C K and Langdon A B 1985 *Plasma Phys. Computer Simul.* (New York: McGraw-Hill)
[11] Verboncoeur J P, Langdon A B and Gladd N T 1995 *Comput. Phys. Commun.* **87** 199–211
[12] Goplen B, Ludeking L, Smithe D and Warren G 1995 *Comput. Phys. Commun.* **87** 54–86
[13] Li Y and Yeh T C 2008 *J. Comput. Electron.* at press, doi:10.1007/s10825-008-0200-z
[14] Fowler R H and Nordheim L W 1928 *Proc. R. Soc.* A **119** 173–81
[15] Lo H Y, Li Y, Chao H Y, Tsai C H, Chen K J, Pan F M, Kuo T C, Liu M and Mo C N 2007 *SID Symp. Dig. (Long Beach, CA)* 586–9
[16] Michaelson H B 1977 *J. Appl. Phys.* **48** 4729–33
[17] He J, Cutler P H and Miskovsky N M 1991 *Appl. Phys. Lett.* **59** 1644–6
[18] Jo S H, Tu Y, Huang Z P, Carnahan D L, Wang D Z and Ren Z F 2003 *Appl. Phys. Lett.* **82** 3520–2